CORA Cork Open Research Archive
Cartlann Taighde Oscailte Chorcaí

UCC Library and UCC researchers have made this item openly available. Please let us know how this has helped you. Thanks!

Title	Slow-fast dynamics in a chaotic system with strongly asymmetric memristive element
Author(s)	Birkoben, Tom; Drangmeister, Moritz; Zahari, Finn; Yanchuk, Serhiy; Hövel, Philipp; Kohlstedt, Hermann
Publication date	2020-06
Original citation	Birkoben, T., Drangmeister, M., Zahari, F., Yanchuk, S., Hövel, P. and Kohlstedt, H. (2020) 'Slow–Fast Dynamics in a Chaotic System with Strongly Asymmetric Memristive Element', International Journal of Bifurcation and Chaos, 30(08), 2050125 (10 pp). doi: 10.1142/S0218127420501254
Type of publication	Article (peer-reviewed)
Link to publisher's version	http://dx.doi.org/10.1142/S0218127420501254 Access to the full text of the published version may require a subscription.
Rights	**© 2020 The Author(s) This is an Open Access article published by World Scientific Publishing Company. It is distributed under the terms of the Creative Commons Attribution 4.0 (CC BY) License which permits use, distribution and reproduction in any medium, provided the original work is properly cited.** https://creativecommons.org/licenses/by/4.0/
Item downloaded from	http://hdl.handle.net/10468/10460

Downloaded on 2021-11-27T11:45:21Z

UCC University College Cork, Ireland
Coláiste na hOllscoile Corcaigh

International Journal of Bifurcation and Chaos, Vol. 30, No. 8 (2020) 2050125 (10 pages)
© The Author(s)
DOI: 10.1142/S0218127420501254

Slow–Fast Dynamics in a Chaotic System with Strongly Asymmetric Memristive Element

Tom Birkoben
Nanoelektronik, Technische Fakultät, Christian-Albrechts-Universität zu Kiel, Kaisertraße 2, 24143 Kiel, Germany
tobi@tf.uni-kiel.de

Moritz Drangmeister
Institut für Theoretische Physik, Technische Universität Berlin, Hardenbergstraße 36, 10623 Berlin, Germany
drangmeister.m@gmail.com

Finn Zahari
Nanoelektronik, Technische Fakultät, Christian-Albrechts-Universität zu Kiel, Kaisertraße 2, 24143 Kiel, Germany
fnz@tf.uni-kiel.de

Serhiy Yanchuk
Institut für Mathematik, Technische Universität Berlin, Straße des 17. Juni 136, 10623 Berlin, Germany
yanchuk@math.tu-berlin.de

Philipp Hövel
School of Mathematical Sciences, University College Cork, Western Road, Cork T12 XF64, Ireland
Institut für Theoretische Physik, Technische Universität Berlin, Hardenbergstraße 36, 10623 Berlin, Germany
philipp.hoevel@ucc.ie

Hermann Kohlstedt
Nanoelektronik, Technische Fakultät, Christian-Albrechts-Universität zu Kiel, Kaisertraße 2, 24143 Kiel, Germany
hko@tf.uni-kiel.de

Received March 18, 2020

We investigate the effect of a memristive element on the dynamics of a chaotic system. For this purpose, the chaotic Chua's oscillator is extended by a memory element in the form of a double-barrier memristive device. The device consists of $Au/NbO_x/Al_2O_3/Al/Nb$ layers and exhibits strong analog-type resistive changes depending on the history of the charge flow. In the obtained system we observe strong changes in the dynamics of chaotic oscillations. The

This is an Open Access article published by World Scientific Publishing Company. It is distributed under the terms of the Creative Commons Attribution 4.0 (CC BY) License which permits use, distribution and reproduction in any medium, provided the original work is properly cited.

Int. J. Bifurcation Chaos 2020.30. Downloaded from www.worldscientific.com
by 77.189.94.155 on 07/22/20. Re-use and distribution is strictly not permitted, except for Open Access articles.

otherwise fluctuating amplitudes of Chua's system are disrupted by transient silent states. Numerical simulations and analysis of the extended model reveal that the underlying dynamics possesses slow–fast properties due to different timescales between the memory element and the base system. Furthermore, the stabilizing and destabilizing dynamic bifurcations are identified that are traversed by the system during its chaotic behavior.

Keywords: Chaotic system; memory; memristive device; memristor; transient silent states.

Int. J. Bifurcation Chaos 2020.30. Downloaded from www.worldscientific.com
by 77.189.94.155 on 07/22/20. Re-use and distribution is strictly not permitted, except for Open Access articles.

1. Introduction

The field of nonlinear dynamics, chaos, and complexity has attracted increasing interest from the point of fundamental science and engineering during the last decades [Schuster & Just, 2005; Strogatz, 2015]. Classical and well-explored nonlinear phenomena form a fundamental scientific repertoire to shed more light on novel interdisciplinary research areas such as complex network systems. To name but a few, this includes spatiotemporal pattern formation in chemical reactions, pulse coupled oscillators, chaotic weather formation or time-delay systems [Epstein & Showalter, 1996; Pikovsky *et al.*, 2003; Yanchuk & Giacomelli, 2017]. Currently, time-varying networks, neuroscience, and social dynamics are areas of intense research efforts in nonlinear science [Sporns, 2011; Osipov *et al.*, 2007; Skarda & Freeman, 1987; Buzsaki, 2006]. Furthermore, nonlinear systems with experimentally observable chaotic signatures have received much attention, as they are widely distributed over many different fields including optical, mechanical and chemical systems [Epstein & Showalter, 1996; Gilet & Bush, 2009; Ievlev *et al.*, 2014; Brzeski *et al.*, 2015; Buzsaki, 2006]. In this context, electronic systems are of particular interest. Rather simple analog circuits allow the study and control of chaos and nonlinear dynamical phenomena. The fast and easy access to system parameters in experiments through the variation of passive elements of the circuit, i.e. resistances, inductances and capacitances, is an effective way to tune the circuit dynamics and to observe the results in real time. The first chaotic circuit was realized by Leon Chua in the 1980s, consisting of three energy storing elements and a nonlinear electronic device. The circuit exhibits a classical period-doubling route to chaos as well as a chaotic double-scroll attractor [Matsumoto, 1984; Chua *et al.*, 1993].

In this paper, we present a realization of Chua's circuit comprising a semiconductor device which shows memrisitve properties [Vaidyanathan & Volos, 2017]. Memristive devices are currently investigated from the perspective of nonvolatile memories and promising devices to mimic basal synaptic mechanisms in neuromorphic circuits [Ielmini & Waser, 2016; Tetzlaff, 2014; Kozma *et al.*, 2012; Adamatzky & Chua, 2014]. In general, a memristive device connects the current I and voltage V nonlinearly. The resistance of such a system depends on a mechanism relating the voltage to a change of an internal state z:

$$I = G(z) \cdot V, \tag{1a}$$

$$\dot{z} = f(z, V). \tag{1b}$$

In its simplest form such a device consists of a metal-insulator-metal capacitor-like structure. Here, an applied voltage can lead to the movement of ions within the insulator, resulting in a change of the resistance [Strukov *et al.*, 2008]. Thus, the history of the applied voltage is connected to the current state of the device. As a result, the current–voltage characteristics or I–V curve of a memristive device exhibits a hysteresis loop. For more details about memristive devices and the underlying physical and chemical mechanisms, see [Ielmini & Waser, 2016].

Recently, a variety of interesting dynamics evoked by the implementation of a memristive device into autonomous oscillators have been found and proposed. The observed dynamics range from the addition of multiple scrolls into a chaotic system [Wang *et al.*, 2017], multiple wings in a 4D system [Zhou *et al.*, 2016; Zhou *et al.*, 2018b] to various attractors in a memrisitve augmented Twin-T Oscillator [Zhou *et al.*, 2018a]. Furthermore, also techniques for the analyses of such systems have been developed further. These include the Flux-Charge Analysis technique which can have advantages regarding the description of the system and its numerical solution [Corinto & Forti, 2017]. However, due to limited availability of robust

Int. J. Bifurcation Chaos 2020.30. Downloaded from www.worldscientific.com
by 77.189.94.155 on 07/22/20. Re-use and distribution is strictly not permitted, except for Open Access articles.

memristive devices, nearly all approaches have in common that they rely on idealistic theoretical memristive models as well as sophisticated circuits mimicking their behavior. Nonetheless, nanoscale memristive devices are promising candidates to improve energy efficiency and increase the integration density of electronic systems. Therefore, in this article we investigate experimentally and theoretically the effects of a more realistic memristive device with asymmetric characteristic curve. Starting from experimental observations (Sec. 2) we propose a detailed mathematical model (Sec. 3) and analyze its dynamics (Sec. 4). In particular, we show how the slow–fast chaotic oscillations emerge.

2. Experiment

Figure 1(a) shows the setup considered in this work. The chaotic circuit as proposed by Leon Chua is extended with a memristive device in parallel to Chua's diode. Therefore, the solid state device superimposes the necessary nonlinearity to drive the chaotic circuit. The current flow through the device discharges the capacitor resulting in an additional negative feedback on it. As the state of the double-barrier memristive device (DBMD) depends strongly on the history of the applied voltages across it, the strength of the additional discharge of the capacitor varies chaotically with time. In Fig. 1(b) a typical I–V curve of the used

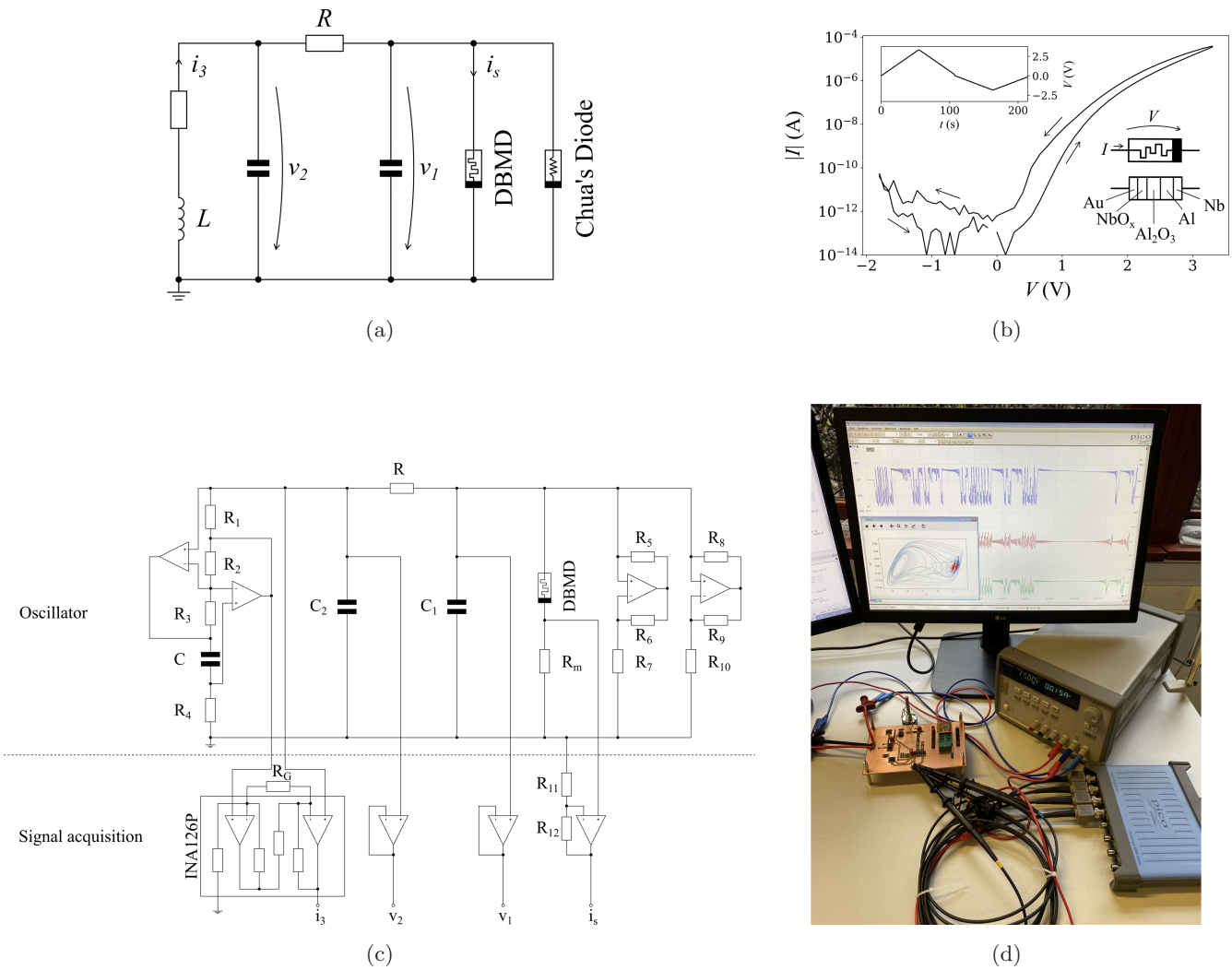

Fig. 1. (a) Setup of Chua's circuit comprising a DBMD. (b) A typical I–V curve of a DBMD. It consists of $Au/NbO_x/Al_2O_3/Al/Nb$ thin layers. As a triangular voltage (inset) is applied to the device, the current characteristics show the typical pinched hysteresis. (c) Experimental realization of the system shown in (a) (the device parameters are given in Appendix A). (d) Photography of the experimental realization.

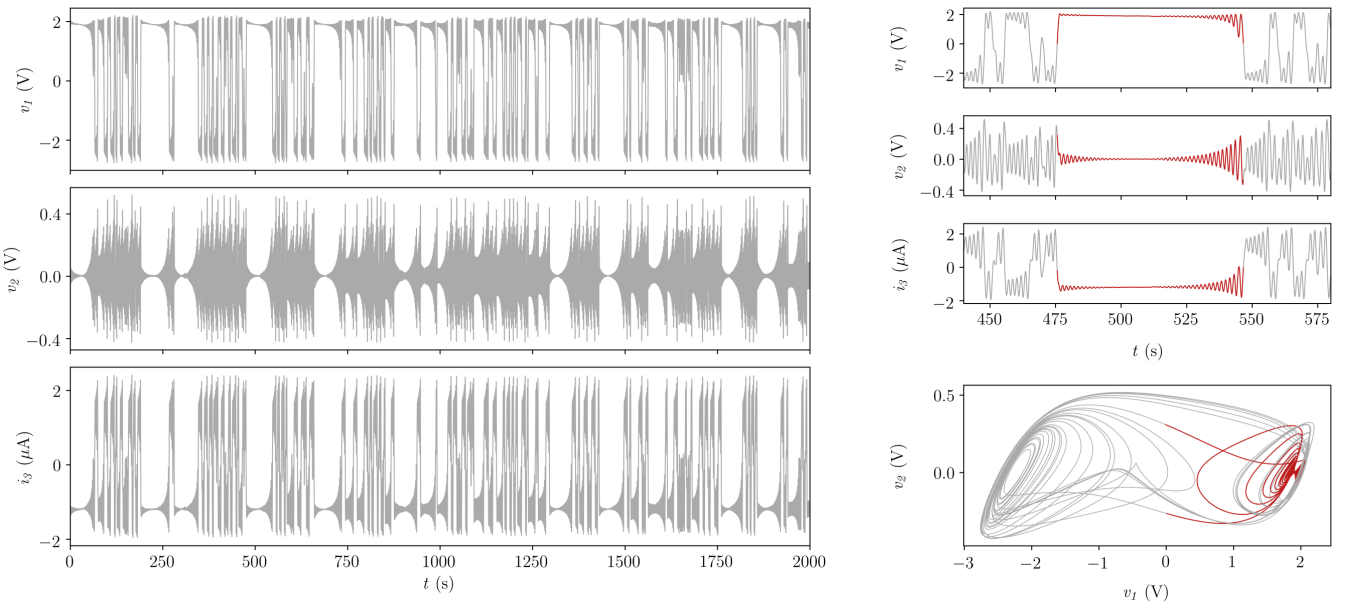

Fig. 2. (a) Time series measurements of Chua's oscillator augmented with a DBMD. (b) Enlargement of one episode of a transient damping. The episode of local damping is marked in red.

Int. J. Bifurcation Chaos 2020.30. Downloaded from www.worldscientific.com
by 77.189.94.155 on 07/22/20. Re-use and distribution is strictly not permitted, except for Open Access articles.

memristive device is shown. The internal structure of the device consists of a $Au/NbO_x/Al_2O_3/Al/Nb$ layer sequence [Hansen *et al.*, 2015; Dirkmann *et al.*, 2016]. The pinched hysteresis, which is characteristic for memristors, is well visible. This means, that the application of a positive voltage changes the state of the device. As a result, the measurable current flow through the device changes depending on the history of the applied voltage. This transition from a high-resistance state (HRS) to a low-resistance state (LRS) becomes visible by applying a positive voltage to the Au electrode in respect to the Nb electrode. The device remains in the LRS after the polarity of the applied voltage switches, but changes its resistance again in an analog fashion to a HRS, if the voltage is beyond a threshold voltage [Hansen *et al.*, 2015]. We emphasize that this kind of device is filament-free, i.e. an interface-based switching is responsible for the pinched hysteresis observed in the I–V curve. Furthermore, the switching is not binary but continuous. Since the change in the state of the memristive element in use is sensitive to the duration of the applied voltage, the intrinsic frequency of Chua's oscillator needs to be adapted. Therefore, the inductance and capacities need to be fairly big to decrease the frequency into the single Hz range. A common strategy in building a huge inductance experimentally is to use a gyrator. In Fig. 1(c) the resulting experimental setup is depicted (for details on the parameters of the devices, see Appendix A). Besides the inductance, Chua's diode is built with active elements as well. Two negative impedance converters built in parallel show the characteristic curve of Chua's diode. The diode is necessary for the autonomous oscillations of the chaotic oscillator. In Fig. 1(d) a photograph of the experimental setup is shown. The small chip with double-barrier memristive devices is located in the top right of the printed circuit board.

The experimental results from the circuit shown in Fig. 1(c) are depicted in Fig. 2. In (a) a long time series measurement of the augmented system is shown. Besides the chaotic oscillations of Chua's oscillator, the system shows transient episodes of local dampening. These episodes occur irregularly during the time evolution of the system. In Fig. 2(b) an enlargement around one of these episodes is shown. The transient dampening is highlighted in red. In the (v_1, v_2) projection of the phase space, the transition to an additional attractor is well visible. The reduction in the oscillation amplitude refers to the transition from the original chaotic attractor to the part of the attractor introduced by the DBMD. In the following, we will present a model to describe and analyze the observed dynamics in the augmented system.

Int. J. Bifurcation Chaos 2020.30. Downloaded from www.worldscientific.com
by 77.189.94.155 on 07/22/20. Re-use and distribution is strictly not permitted, except for Open Access articles.

3. Model

Since the memristive device is implemented experimentally in parallel to Chua's diode, the voltage drop across the device is equal to the state variable v_1 of the original chaotic oscillator. Therefore, the current flow through the DBMD discharges the capacitor and functions as a negative feedback to the first state-variable v_1. The modified equations of Chua's system augmented by the memory element are as follows:

$$\dot{v}_1 = \frac{1}{C_1}\left(\frac{v_2 - v_1}{R} - f(v_1) - i_s(v_s, z)\right), \quad (2a)$$

$$\dot{v}_2 = \frac{1}{C_2}\left(\frac{v_1 - v_2}{R} - i_3\right), \quad (2b)$$

$$\dot{i}_3 = -\frac{1}{L}v_2, \quad (2c)$$

with Chua's diode modeled as a piecewise-linear function:

$$f(v_1) = m_0 v_1 + \frac{m_1 - m_0}{2}(|v_1 + B_p| - |v_1 - B_p|). \quad (3)$$

The DBMD consists of a multilayer structure of different materials [see Fig. 1(b)], which can be interpreted in terms of an equivalent circuit as depicted in Fig. 3. The metal semiconductor transition is modeled as a Schottky contact followed by a tunnel barrier. Thus, the equations describing the equivalent circuit are as follows:

$$\dot{v}_e = \frac{1}{C_e}\left(i_s(v_s, z) - \frac{v_e}{R_e(z)}\right), \quad (4a)$$

$$\dot{v}_t = \frac{1}{C_t}(i_s(v_s, z) - i_t(v_t, z)), \quad (4b)$$

$$\dot{z} = -\frac{\hat{Z}\omega(z)}{e^{\varphi_a(v_1, z)}} \sinh\left(\frac{v_r(v_1, v_s, z) + v_e - V_c}{V_e}\right), \quad (4c)$$

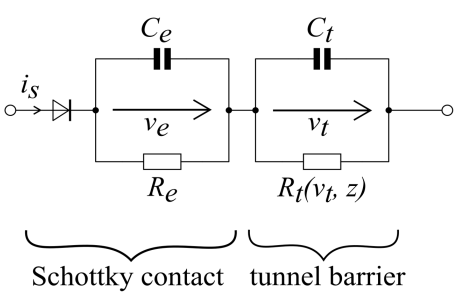

Fig. 3. Equivalent circuit of the DBMD.

where v_e and v_t are internal voltage variables as shown in Fig. 3. The memory component of the DBMD is represented through the state variable z, which refers to the average ion-position inside the active layer, that is the NbO_x solid-state electrolyte. During the switching oxygen vacancies move and consequently decrease and increase the potential on the interface at the Schottky contact and the tunnel barrier, respectively [Solan *et al.*, 2017]. The voltage over the Schottky contact is $v_s = v_1 - v_e - v_t$ and leads to the total current $i_s(v_s, z)$ through the device as:

$$i_s(v_s, z) = I_s \exp\left(-\varphi_s(z) - \alpha_f\sqrt{\frac{|v_s| - v_s}{\alpha_s V_\vartheta}}\right) \times \left[\exp\left(\frac{v_s}{n(z)V_\vartheta}\right) - 1\right], \quad (5)$$

with $\varphi_s(z)$ as the state-dependent normalized Schottky-barrier height, $n(z)$ as an ideality factor and α_f as a fitting parameter for the Schottky-effect denoted by the normalized Schottky-barrier thickness α_s. The amplitude of the current I_s scales the total current depending on the temperature and device area, respectively [Solan *et al.*, 2017]. The closed system (2)–(5) describes the dynamics of the complete circuit augmented with a DBMD (for additional information about the model see Appendix B).

As one can observe from Fig. 4, the results of the numerical simulation of the closed system are in agreement with the measurement data (compare Fig. 2). The purely chaotic dynamics are interrupted by relatively long time intervals of almost constant voltages and currents. After a period nearly without any oscillations, an onset of the local oscillations follows. Again, the local oscillations are amplified until the trajectory switches to the opposite side of the characteristic double-scroll attractor. The strong diode-like characteristic of the DBMD diminishes the influence of itself on the other side of the chaotic double-scroll attractor. This results in the asymmetric change of the system behavior. The numerical solution demonstrates clearly the role of the internal state variable of the DBMD.

In Fig. 5(a) the time series for one typical transient silent state (TSS) is shown in the (v_1, v_2, z) projection of the phase space. The decrease of the internal state z can be observed over time, which leads to a higher conductance of the device and a damping of the oscillations. It is followed by a steep

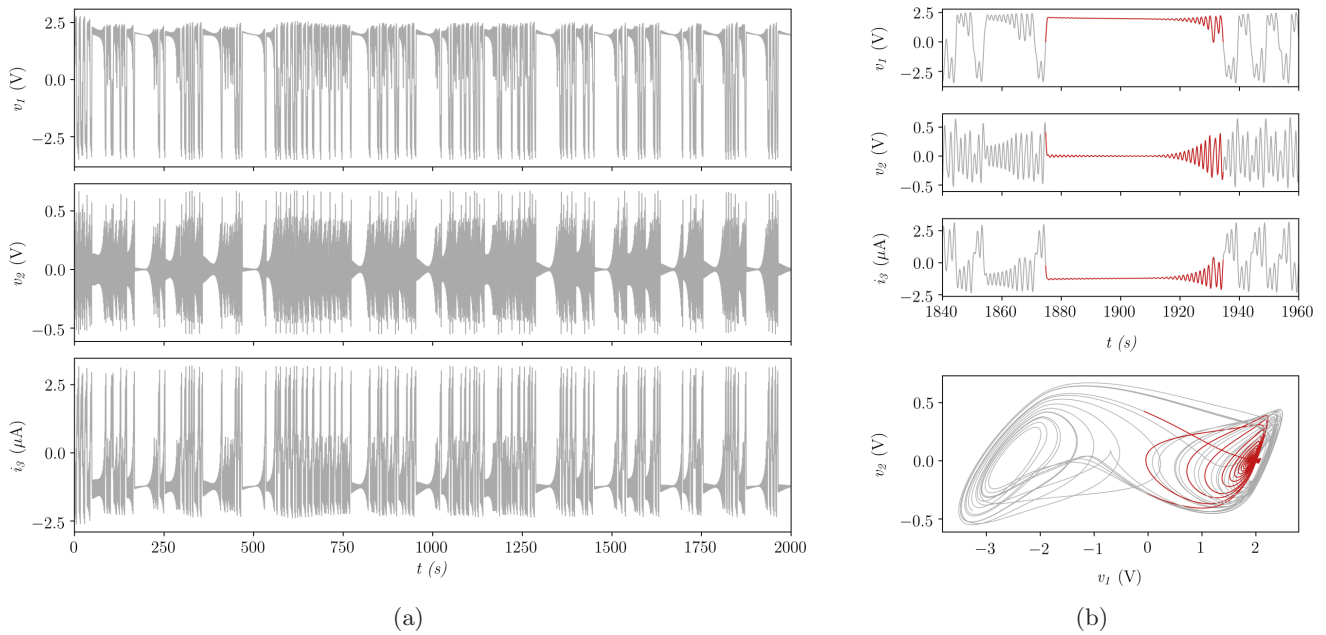

Fig. 4. (a) Numerical results of Chua's oscillator augmented with a DBMD. (b) Enlargement of one episode of a transient damping (red).

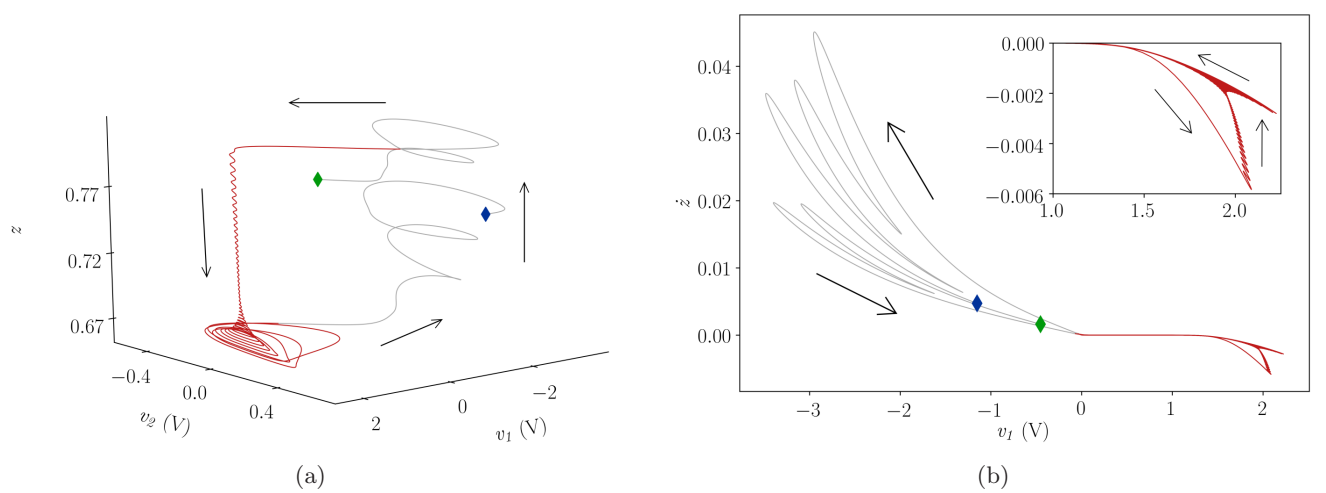

Fig. 5. (a) (v_1, v_2, z) projection of phase space of one episode of damping and following amplification. Green and blue diamonds mark the start and end of the trajectory, respectively. (b) Time derivative of z in dependence on v_1, for the same time interval as in panel (a).

increase when the resuming chaotic oscillations lead to a negative voltage over the memristive device. The derivative of z is depicted in Fig. 5.

4. Slow–Fast Motion

In the following, we show that the chaotic dynamics with TSS events can be understood as a slow–fast motion with the slowest timescale governed by the memory z. More specifically, the variable z can be considered as a control parameter for the remaining faster variables, i.e. $\dot{z} = 0$ [Dumortier *et al.*, 1996; Krupa *et al.*, 1997; Desroches *et al.*, 2012; Kuehn, 2015; Jardon-Kojakhmetov & Kuehn, 2019].

Figure 6(a) shows a bifurcation diagram for v_1 in dependence on z as a control parameter. For the experimentally chosen value $R = 1.6\,\mathrm{M\Omega}$, the fast dynamics possess a stable stationary state $(v_e(z), v_t(z), v_1(z), v_2 = 0, i_3(z))$ for all values of z in the interval $0.71 < z < 0.86$, shown by the solid blue line in Fig. 6(a). At the boundaries, $z = 0.71$ and $z = 0.86$, the branch becomes unstable in subcritical Hopf bifurcations. This set [solid blue line

Int. J. Bifurcation Chaos 2020.30. Downloaded from www.worldscientific.com by 77.189.94.155 on 07/22/20. Re-use and distribution is strictly not permitted, except for Open Access articles.

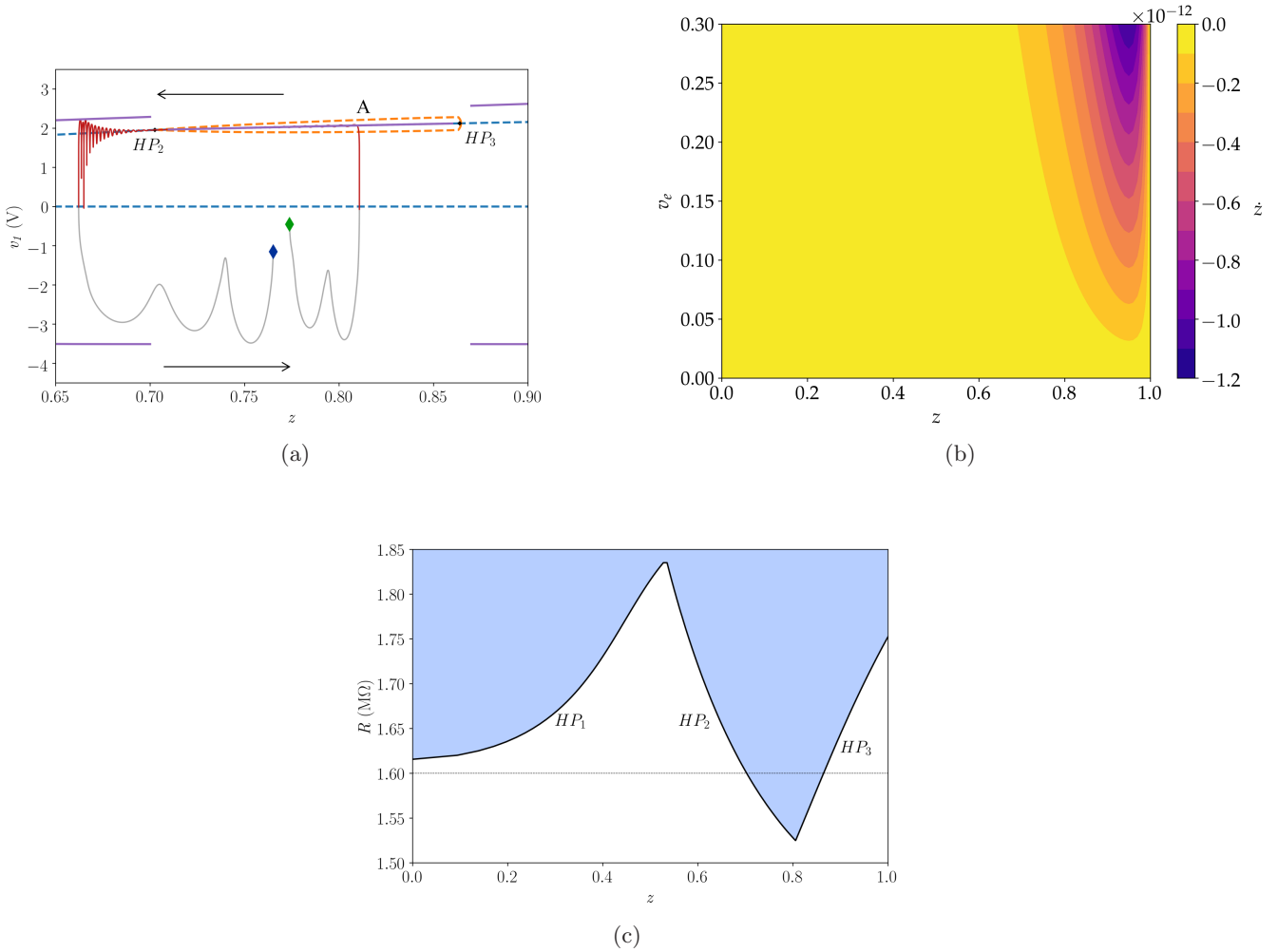

Fig. 6. (a) Bifurcation diagram for v_1 over control parameter z with stationary solutions in blue, periodic solutions in orange and chaotic solutions in purple (stable = solid line, unstable = dashed line). The trajectory follows the arrows. (b) $\dot{z}$ as a function of z and v_e for positive values of v_1. (c) Position of the Hopf bifurcation points (HP) parametrized by R if z is varied as a control parameter. The blue shaded area shows where a stable branch exists in the solution. During the experiment R is fixed at 1.6 MΩ (dashed, horizontal line).

stable critical manifold [Kuehn, 2015], and the trajectories of the full system are attracted to this manifold on the fast timescale. Being close to the manifold, the dynamics are then governed in Fig. 6(a)] is called the by the single scalar equation (4c) for the z variable with all fast variables being confined to the manifold. With $v_1 > 0$ Eq. (4c) reduces to:

$$\dot{z} = -\frac{\hat{Z}\omega(z)}{e^{\varphi_{a1}+z(\varphi_{a0}-\varphi_{a1})}} \sinh\left(\frac{v_e - V_c}{V_e}\right) \qquad (6)$$

as $v_r(v_1 > 0, v_s, z) = 0$ and $\varphi_a(v_1 > 0, z) = \varphi_{a1} + z(\varphi_{a0} - \varphi_{a1})$. From the differential equation (6) it can be seen that z decreases on the slow manifold as positive values for v_1 lead to a negative sign of the derivative [cf. Fig. 6(b)]. This corresponds to motion along the manifold to the left.

These multiscale arguments explain parts of the dynamics observed in the full system and are shown in Fig. 6(a). Once the trajectory is attracted to the slow manifold [point A in Fig. 6(a)], the TSS episode starts and the memory variable z decreases slowly until it reaches the Hopf point HP_2 at $z = 0.71$. Beyond this point, the slow manifold becomes unstable and the trajectory exhibits amplified oscillations, while z still decreases further. When the oscillations become sufficiently large, the orbit leaves the neighborhood of the slow manifold and the TSS episode ends. In fact, we observe here a classical delayed stability loss, when the orbits

Int. J. Bifurcation Chaos 2020.30. Downloaded from www.worldscientific.com
by 77.189.94.155 on 07/22/20. Re-use and distribution is strictly not permitted, except for Open Access articles.

Int. J. Bifurcation Chaos 2020.30. Downloaded from www.worldscientific.com
by 77.189.94.155 on 07/22/20. Re-use and distribution is strictly not permitted, except for Open Access articles.

remain for certain time close to the unstable part of the slow manifold [Dumortier *et al.*, 1996; Krupa *et al.*, 1997; Desroches *et al.*, 2012; Kuehn, 2015; Jardon-Kojakhmetov & Kuehn, 2019].

After the TSS has terminated, the voltages v_1, v_e, and v_t decrease and the variable z accelerates and approaches the fast timescale [cf. Fig. 5(b)] for the gradient $\dot{z}$ along the trajectory. In this way, a slow setting to a LRS and a faster reset to a HRS drives the slow–fast dynamics behind the TSS.

Figure 6(c) shows the positions of the Hopf points on the slow manifold. These determine the length of the TSS phases, depending on R. See for instance, the intersection of the dashed line at $R = 1.6\,\mathrm{M}\Omega$ with the stable area marked in blue. The stable branch can be seen to expand with increasing R, until the stability becomes independent of z as HP_1 and HP_2 collide. For decreasing R, the stable branch shrinks and vanishes with HP_2 and HP_3.

5. Conclusion

In summary, we have described the influence of a new solid state memory device on a model system exhibiting chaotic dynamics to study the influence of memory on chaos. Interestingly, the intrinsic memory of the DBMD has a stabilizing and ordering effect on the otherwise purely chaotic motions of the system. The experimental observation as well as the subsequent theoretical treatment reveal the underlying dynamics. We have observed that the memory acts on the slowest timescale, and thus, it can be considered as an intrinsic slowly-changing bifurcation parameter. In particular, when the fast chaotic motion of the system is interrupted by a TSS, the dynamics can be considered as a steady state, which is adiabatically changing with the slow variation of the memory. Then, the chaotic oscillations are dampened until the stability changes. Such a change occurs when the memory reaches a threshold, and a Hopf bifurcation of the fast system leads to amplification of chaotic oscillations. As the memristive device in use has two timescales for the set and reset of the resistive states, this damping and successive amplification is driven by these slow–fast dynamics. Although this study is restricted to an electronic system, the observed behavior and general dynamical changes might be found in a broader range of systems. The occurrence of transiently stable and ordered behavior in otherwise highly nonlinear or chaotic trajectories might be related to dynamic bifurcations as an intrinsic memory element of these systems changes its state. The sequence of these transient states is primarily driven by the underlying chaotic motions but the duration and recovery depend strongly on the characteristic timescales of this memory element. Speaking in more general terms it is driven by the time needed to adapt to a new input. The considered model is a practically important example of a system with slow–fast dynamics, where such theoretical multiscale methods as singular perturbation theory or averaging [Dumortier *et al.*, 1996; Krupa *et al.*, 1997; Desroches *et al.*, 2012; Kuehn, 2015; Jardon-Kojakhmetov & Kuehn, 2019] can be further applied for more detailed analysis.

Acknowledgments

The authors acknowledge financial support by Deutsche Forschungsgemeinschaft (DFG, German Research Foundation), projects RU2093 (T. Birkoben, F. Zahari and H. Kohlsted), 411803875 (S. Yanchuk) and Collaborative Research Center 910 (M. Drangmeister and P. Hövel).

References

Adamatzky, A. & Chua, L. [2014] *Memristor Networks*, Vol. 1 (Springer).

Buzsaki, G. [2006] *Rhythms of the Brain* (Oxford University Press, Oxford, NY).

Brzeski, P., Kapitaniak, T. & Perlikowski, P. [2015] "Analysis of transitions between different ringing schemes of the church bell," *Int. J. Impact Engin.* **85**, 57–66.

Chua, L. O., Wu, C. W., Huang, A. & Zhong, G.-Q. [1993] "A universal circuit for studying and generating chaos. I. Routes to chaos," *IEEE Trans. Circuits Syst.-I*: *Fund. Th. Appl.* **40**, 732–744.

Corinto, F. & Forti, M. [2017] "Memristor circuits: Bifurcations without parameters," *IEEE Trans. Circuits Syst.-I*: *Reg. Papers* **64**, 1540–1551.

Desroches, M., Guckenheimer, J., Krauskopf, B., Kuehn, C., Osinga, H. M. & Wechselberger, M. [2012] "Mixed-mode oscillations with multiple time scales," *SIAM Rev.* **54**, 211–288.

Dirkmann, S., Hansen, M., Ziegler, M., Kohlstedt, H. & Mussenbrock, T. [2016] "The role of ion transport phenomena in memristive double barrier devices," *Scient. Rep.* **6**, 35686.

Dumortier, F. & Roussarie, R. [1996] *Canard Cycles and Center Manifolds* (American Mathematical Society).

Int. J. Bifurcation Chaos 2020.30. Downloaded from www.worldscientific.com
by 77.189.94.155 on 07/22/20. Re-use and distribution is strictly not permitted, except for Open Access articles.

Epstein, I. R. & Showalter, K. [1996] "Nonlinear chemical dynamics: Oscillations, patterns, and chaos," *J. Phys. Chem.* **100**, 13132–13147.

Gilet, T. & Bush, J. W. M. [2009] "Chaotic bouncing of a droplet on a soap film," *Phys. Rev. Lett.* **102**, 014501.

Hansen, M., Ziegler, M., Kolberg, L., Soni, R., Dirkmann, S., Mussenbrock, T. & Kohlstedt, H. [2015] "A double barrier memristive device," *Scient. Rep.* **5**, 13753.

Ielmini, D. & Waser, R. (eds.) [2016] *Resistive Switching*: *From Fundamentals of Nanoionic Redox Processes to Memristive Device Applications* (Wiley-VCH, Weinheim).

Ievlev, A. V., Jesse, S., Morozovska, A. N., Strelcov, E., Eliseev, E. A., Pershin, Y. V., Kumar, A., Shur, V. Y. & Kalinin, S. V. [2014] "Intermittency, quasiperiodicity and chaos in probe-induced ferroelectric domain switching," *Nat. Phys.* **10**, 59–66.

Jardon-Kojakhmetov, H. & Kuehn, C. [2019] "A survey on the blow-up method for fast–slow systems," arXiv:1901.01402 [math].

Kozma, R., Pino, R. E. & Pazienza, G. E. (eds.) [2012] *Advances in Neuromorphic Memristor Science and Applications*, Vol. 4, Springer Series in Cognitive and Neural Systems (Springer, Dordrecht).

Krupa, M., Sandstede, B. & Szmolyan, P. [1997] "Fast and slow waves in the FitzHugh–Nagumo equation," *J. Diff. Eqs.* **133**, 49–97.

Kuehn, C. [2015] *Multiple Time Scale Dynamics*, Vol. 191 (Springer-Verlag GmbH).

Matsumoto, T. [1984] "A chaotic attractor from Chua's circuit," *IEEE Trans. Circuits Syst.* **31**, 1055–1058.

Osipov, G. V., Kurths, J. & Zhou, C. [2007] *Synchronization in Oscillatory Networks*, Springer Series in Synergetics (Springer, Berlin).

Pikovsky, A., Rosenblum, M. & Kurths, J. [2003] *Synchronization*: *A Universal Concept in Nonlinear Sciences*, Vol. 12 (Cambridge University Press).

Schuster, H. G. & Just, W. [2005] *Deterministic Chaos*: *An Introduction*, 4th edition (Wiley-VCH, Weinheim).

Skarda, C. A. & Freeman, W. J. [1987] "How brains make chaos in order to make sense of the world," *Behav. Brain Sci.* **10**, 161–173.

Solan, E., Dirkmann, S., Hansen, M., Schroeder, D., Kohlstedt, H., Ziegler, M., Mussenbrock, T. & Ochs, K. [2017] "An enhanced lumped element electrical model of a double barrier memristive device," *J. Phys. D* **50**, 195102.

Sporns, O. [2011] *Networks of the Brain* (MIT Press, Cambridge, Mass.).

Strogatz, S. H. [2015] *Nonlinear Dynamics and Chaos*: *With Applications to Physics, Biology, Chemistry, and Engineering*, 2nd edition (Westview Press, a member of the Perseus Books Group, Boulder, CO).

Strukov, D. B., Snider, G. S., Stewart, D. R. & Williams, R. S. [2008] "The missing memristor found," *Nature* **453**, 80–83.

Tetzlaff, R. (ed.) [2014] *Memristors and Memristive Systems* (Springer, NY).

Vaidyanathan, S. & Volos, C. (eds.) [2017] *Advances in Memristors, Memristive Devices and Systems*, Studies in Computational Intelligence, Vol. 701 (Springer International Publishing, Cham).

Wang, C., Liu, X. & Xia, H. [2017] "Multi-piecewise quadratic nonlinearity memristor and its $2N$-scroll and $2N + 1$-scroll chaotic attractors system," *Chaos* **27**, 033114.

Yanchuk, S. & Giacomelli, G. [2017] "Spatio-temporal phenomena in complex systems with time delays," *J. Phys. A*: *Math. Theor.* **50**, 103001.

Zhou, L., Wang, C. & Zhou, L. [2016] "Generating hyperchaotic multi-wing attractor in a 4D memristive circuit," *Nonlin. Dyn.* **85**, 2653–2663.

Zhou, L., Wang, C., Zhang, X. & Yao, W. [2018a] "Various attractors, coexisting attractors and antimonotonicity in a simple fourth-order memristive twin-t oscillator," *Int. J. Bifurcation and Chaos* **28**, 1850050-1–18.

Zhou, L., Wang, C. & Zhou, L. [2018b] "A novel no-equilibrium hyperchaotic multi-wing system via introducing memristor: No-equilibrium hyperchaotic memristive multi-wing system," *Int. J. Circuit Th. Appl.* **46**, 84–98.

Appendix A
Devices and Values

According to Table 1 the values of the components are used to build Chua's oscillator. Since the characteristic slow timescale of the DBMD is on the order of seconds, the capacitances C_1 and C_2 as well as the used inductance L are chosen to bring the chaotic oscillations into the single Hz range. To

Table 1. Values of the components used in the experiment.

Variable	Value	Variable	Value
R	1.6 MΩ	R_9	22 MΩ
R_1	1 kΩ	R_G	100 kΩ
R_2	100 Ω	R_m	1 kΩ
R_3	10 kΩ	R_{10}	3.3 MΩ
R_4	1.82 MΩ	R_{11}	100 Ω
R_5	250 kΩ	R_{12}	100 kΩ
R_6	250 kΩ	C	0.47 μF
R_7	2.5 MΩ	C_1	0.047 μF
R_8	22 MΩ	C_2	0.47 μF

decrease the occurring currents, the resistance R is increased. The huge inductance is implemented experimentally through a gyrator. The recordings of the state variables are done using a *PicoScope 3000 Series*. Furthermore, to decrease the influence of the measurement on the circuit, unity gain followers are built with JFET general purpose operational amplifiers (TL074 and TL071). The simulations are carried out using *Python 3.6* running the *scipy* library.

Appendix B

Additional Information about the Model

The following set of equations describes the ion motions inside the DBMD as well as the increase and decrease of the interfacial energy barrier heights:

$$\omega(z) = (1 - 2\omega_0)[1 - (2z - 1)^p] + \omega_0, \tag{B.1a}$$

$$\varphi_a(v_1, z) = \sigma(v_1)[\varphi_{a1} + z(\varphi_{a0} - \varphi_{a1}) - \varphi_{ar}] + \varphi_{ar}, \tag{B.1b}$$

$$v_r(v_1, v_s, z) = \sigma(-v_1)v_s(1 - z), \tag{B.1c}$$

$$\varphi_s(z) = \varphi_{s0} + z(\varphi_1 - \varphi_0), \tag{B.1d}$$

$$n(z) = n_0 + z(n_1 - n_0), \tag{B.1e}$$

$$R_e(z) = R_{e0} + z(R_{e1} - R_{e0}), \tag{B.1f}$$

$$i_t(v_t, z) = \frac{I_t g(-v_t, z) - g(v_t, z)}{\alpha_t(z)^2}, \tag{B.1g}$$

$$g(v_t, z) = \varphi_t(v_t) e^{-\alpha_t(z)\sqrt{\varphi_t(v_t)}}, \tag{B.1h}$$

$$\varphi_t(v_t) = \varphi_{t0} + \frac{v_t}{2V_\vartheta}, \tag{B.1i}$$

$$\alpha_t(z) = \alpha_{t0} + z(\alpha_{t1} - \alpha_{t0}), \tag{B.1j}$$

$$\sigma(x) = \begin{cases} 1 & \text{for } x > 0, \\ 0 & \text{otherwise.} \end{cases} \tag{B.1k}$$

The used values for the simulation are as follows:

Table 2. Parameters and constants of the DBMD, rounded on three digits.

Variable	Value	Variable	Value
L	85 540 H	φ_{a0}	26.305
m_0	$-3.545 \cdot 10^{-7}$	φ_{ar}	30.173
m_1	$-7.03 \cdot 10^{-7}$	ω_0	$1 \cdot 10^{-4}$
B_P	1.957	φ_{s0}	27.079
C_e	$1.74 \cdot 10^{-13}$ F	φ_{s1}	34.815
C_t	$2.07 \cdot 10^{-13}$ F	n_0	2.9
V_c	$1 \cdot 10^{-4}$ V	n_1	4.1
V_e	0.323 V	R_{e0}	200 kΩ
I_s	1.081 A	R_{e1}	510 kΩ
I_t	4.326 A	φ_{t0}	108.314
α_f	−1.25	V_ϑ	0.026 V
α_s	3.77	p	12
$\hat{Z}$	0.64 THz	α_{t0}	1.812
φ_{a1}	36.749	α_{t1}	2.026

Int. J. Bifurcation Chaos 2020.30. Downloaded from www.worldscientific.com
by 77.189.94.155 on 07/22/20. Re-use and distribution is strictly not permitted, except for Open Access articles.